

# Preparation of self-organized nanotubes on Ti-50Ta alloy by anodic oxidation

JUN LI<sup>a</sup>, XIANJIN YANG<sup>a,b,\*</sup>, ZHENDUO CUI<sup>a</sup>, SHENGLI ZHU<sup>a,b</sup>

<sup>a</sup> School of Materials Science and Engineering, Tianjin University, Tianjin 300072, China

<sup>b</sup> Tianjin Key Laboratory of Composite and Functional Materials, Tianjin 300072, China

The present work demonstrates the self-organized nanotube oxide layers on Ti-50Ta alloy by anodic oxidation. Highly ordered nanotube layers can be formed on the alloy under different anodization parameters. In aqueous solution containing glycerol and  $\text{NH}_4\text{F}$ , the diameter of the nanotubes can be strongly influenced by the applied potential, while length of the nanotubes is determined by the electrolyte temperature and anodization time. Nanotubes with hexagonal arrangement are formed under appropriate condition. Each nanotube exhibits hexagonal prism shape and is surrounded by six others. The amorphous oxide phase of the nanotubes transforms to anatase and rutile phases after heat treatment.

(Received July 15, 2011; accepted August 10, 2011)

**Keywords:**  $\text{TiO}_2$  nanotube, Ti-50Ta alloy, Self-organized

## 1. Introduction

Over the last decades titanium dioxide, due to its specific properties, has been widely investigated for plenty of applications, such as photocatalysis, photocleavage, dye-sensitized solar cells and the biomedical field [1-4]. In 1999, the pioneering work of Zwillling et al. [5] successfully showed  $\text{TiO}_2$  nanotube formation on an anodized Ti surface in HF-based electrolyte. The nanotube-array was subsequently obtained in various electrolytes, such as aqueous or non-aqueous,  $\text{F}^-$ -containing or  $\text{F}^-$ -free, organic or inorganic acidic electrolytes [6, 7]. The nanotubular layers had a thickness ranged from approximately 500 nm to 200  $\mu\text{m}$  in these experiments. Self-organized oxide layers structure can be formed on pure valve metals [8-11] and their alloys [12-14]. Most of the self-organized nanotubular structures consist of either uniform or continuous size distribution. In addition, multiscale self-organized oxide nanotube arrays with two distinct sizes and geometries were also fabricated on some alloys. Although the detailed mechanism for the two-size-scale structures is so far unclear, it is confirmed that this two-size-scale structures could be resulted in by many factors, such as the composition and phase structures of the alloys [15-18].

The formation of nanotubular oxide structures on Ti-Ta alloys with different compositions had been investigated in inorganic electrolyte containing HF. Compared with the other compositions, nanotubes on Ti-50Ta alloy exhibited a different structure: the nanotubes layer consists of two distinct diameter tubes - larger tubes are surrounded by several smaller tubes [19]. In addition,

it was reported that the Ti-50Ta alloy has the potential for biomedical application due to its low elastic modulus and high strength [20]. The surface microstructure of the implants is important for long-term cultivation, hence the surface modification of Ti-Ta alloys should be considered. The self-organized anodic oxidation is a kind of efficient way to improve the surface bioactivity of Ti-Ta alloys.

In the present work, we prepared highly ordered nanotube layers on Ti-50Ta alloy by electrochemical anodization in aqueous organic electrolyte. The influence of process parameters, such as anodization time, voltage and the temperature of electrolyte, on nanotube dimensions was also investigated.

## 2. Experimental

Binary alloy ingots were prepared by melting high purity Ti (99.6 %) and 50 wt.% Ta (99.9 %) using a vacuum arc melting furnace. Heat treatment was subsequently performed at 1400 °C for 6 h in an argon atmosphere to homogenize the microstructure of the alloy. The samples with a typical dimension of  $10 \times 10 \times 0.6 \text{ mm}^3$  were prepared by wire-electrode cutting the ingots.

The samples were ground with emery papers up to 5000 #, followed by successively ultrasonic cleaning in ethanol for 5 min, rinsing with deionized water and drying in air. Electrochemical experiments were carried out with a two-electrode system. The working electrode was the ground sample, leaving an area of approximate  $0.5 \text{ cm}^2$  exposed to the anodizing electrolyte which composed of 10:90 vol.% of  $\text{H}_2\text{O}$ :  $\text{C}_3\text{H}_8\text{O}_3$  containing 0.3 M  $\text{NH}_4\text{F}$ . A

platinum plate served as the counter electrode. The distance between two electrodes was 2.5 cm. Electrochemical experiments were performed using a high-voltage sourcemeter (Keithley 2400, USA) at designed temperatures. The potential was first swept from open-circuit potential (OCP) to a designed potential at a rate of 50 mV/s, followed by holding the designed potential for different time. After the treatment, the samples were rinsed with deionized water and dried in air before annealed at 450 °C, 600 °C and 750 °C respectively for 2 h.

The morphology and structure of the nanotubular layer were characterized using a field-emission scanning electron microscope (FE-SEM S4800; Hitachi, Japan). The cross-sectional and bottom views were taken from mechanically scratched samples where some pieces flaked off and were upside down. The crystal structure of the samples was identified using an X-ray diffraction (XRD; RIGAKU/DMAX2500, Japan).

### 3. Results and discussion

Fig. 1 shows SEM images of top and bottom view of the formed layer on Ti-50Ta alloy anodized for different time at ambient temperature (approximate 20 °C) under 20 V in 10:90 vol.% of H<sub>2</sub>O: C<sub>3</sub>H<sub>8</sub>O<sub>3</sub> containing 0.3 M NH<sub>4</sub>F (the cross-sectional images are shown in the insets). A top nanoporous structure was formed during the first two hours with the diameter of about 20 and thickness of about 85 nm, as shown in Fig. 1 (a1, b1). Cross-sectional images show that nanotubes are formed under the top porous layer. This behavior of a top nanoporous and an underneath nanotube layer had recently been reported for Ti-Nb alloys [15]. After anodized for 4 h, the top nanoporous layer was completely dissolved. As a result the underneath honeycomb-like nanotube layer could be observed from the top as shown in Fig. 1 (c1). The thickness of underneath nanotube layer was approximate 4.2 μm. At the same time, nanotubes with different height levels can be observed due to the different chemical dissolution rate. After 40 h, the thickness of nanotube layer increased up to approximate 11.6 μm and the surface dissolved more seriously, as shown in Fig. 1 (d1). The side-walls of the tubes are quite smooth, which is different from the samples on which some ripples appeared due to the current oscillations [6, 16].

Fig. 1 (a2, b2, c2, d2) shows the bottoms microstructure of nanotube with ordered arrangements. As the anodization time prolonged from 1 to 40 h, the bottom

diameter of the nanotube increased from 51 to 72 nm. The space of diameter enlarging was provided following the mechanism that some of nanotubes with slower growth stopped growing and were finally buried, as shown in Fig. 1 (a2). Tsuchiya et. al. reported the growth competition between nanotubes with different growth rate [17]. There was a dark area in the center of each nanotube, as shown in Fig. 1 (d2), conforming that the as-formed nanotubes were hollow. Therefore the wall thickness of nanotubes at the bottom could be calculated by the bottom part excluding the dark area in each nanotube. The mean wall thickness of the nanotubes at the top is smaller than that of those at the bottom (diameter,  $d_{top}$ = 7.6 nm and  $d_{bottom}$ =16.5 nm) which results from constant chemical etching of the tube walls in the fluoride-containing electrolyte [19]. In addition, the bottom of the as-formed nanotubes presents hexagonal arrangement, which is mainly attributed to the close-packed structure of nanotubes. It seems that the nanotubes presents hexagonal bottom in the whole growth stage. One hexagonal nanotube is surrounded by six others as shown in Fig. 1 (c2, d2).

TiO<sub>2</sub> nanotubes possess more specific area and stronger adsorption ability compared with other forms of TiO<sub>2</sub> [21]. The increase of tube length can improve Ti-50Ta alloy in photocatalytic application. The dependence curve of nanotube length at ambient temperature and 50 °C on anodization time at 20 V is shown in Fig. 2. It is worthy to note that the length of nanotubes formed at 50 °C is more than two times longer than that formed at ambient temperature. The nanotube growth rate in the first hour was relative faster than that in other time, which was about 30 nm / min at ambient temperature and 100 nm / min at 50 °C, respectively. The length of nanotubes anodized at 20 V under ambient temperature increased from approximate 1.8 μm anodized for 1 h to 6.2 μm anodized for 5 h, and then dropped to 5 μm anodized for 6 h. This indicates that the growth steady-state can be obtained where nanotube growth rate is equal to nanotube dissolution rate [22], whereas the length increased from approximate 5.8 to 15.5 μm when anodized at 50 °C. The length of nanotubes formed at 50 °C for 1 h is higher than that formed at ambient temperature for 6 h. It is believed that the growth of nanotubes needs three indispensable simultaneously occurring processes: surface oxidation, dissolution of formed oxidation and chemical dissolution of both substrate and oxidation [10, 21]. We can deduce that higher temperature would create a better atmosphere for ion diffusion and then accelerate the growth of nanotubes.

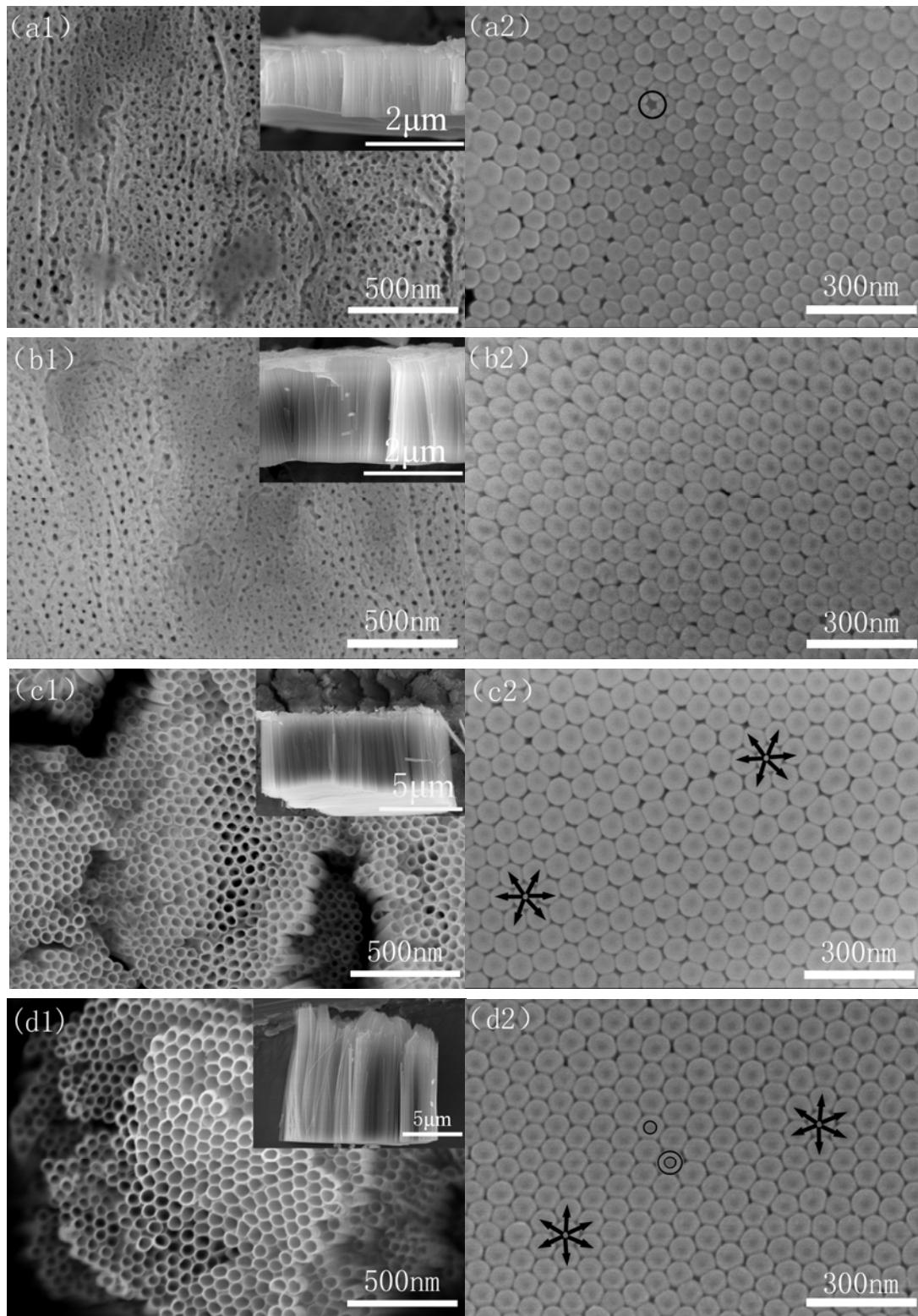


Fig. 1. Top-view (cross-sectional view in insets) and bottom-view SEM images of oxide layers formed on Ti-50Ta (a) 1 h; (b) 2 h; (c) 4 h; (d) 40 h by anodization at 20 V in 10:90 vol.% of  $H_2O$ :  $C_3H_8O_3$  containing 0.3 M  $NH_4F$ . (The circle in (a2) shows the nanotubes with slower growth, the snowflake-shape arrows in (c2) and (d2) show the six-square-column shape bottom, and the circles in (d2) show the dark area and the wall thickness of nanotubes at the bottom).

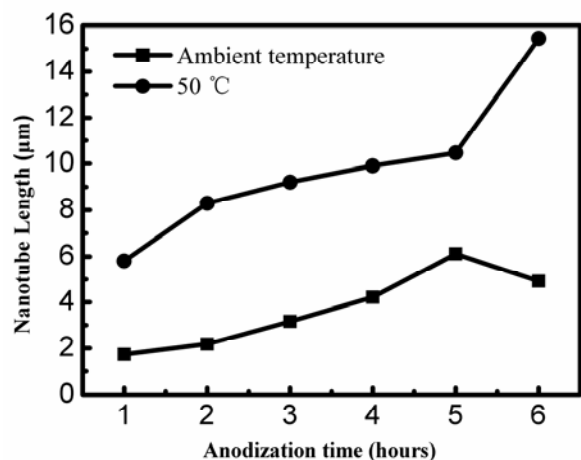


Fig. 2. Dependence of nanotube length at ambient temperature and 50 °C on anodization time at 20 V.

Fig. 3 shows the top and bottom view of the resulting layers anodized at 50 °C on Ti-50Ta under different potential in 10:90 vol.% of H<sub>2</sub>O: C<sub>3</sub>H<sub>8</sub>O<sub>3</sub> containing 0.3 M NH<sub>4</sub>F for 1 h (the cross-sectional images are shown in the insets). A surface layer with most of nanotubes and few of nanoporous regions was formed on Ti-50Ta alloy under 50 °C at 10 V, as shown in Fig. 3 (a1). With increasing potential, the nanotubes region reduced and nanoporous region enlarged. When the potential increased to 40 V, the surface layer became nanoporous structure completely. As voltage changes, the state that the cracks on the top surface disappeared gradually also illustrates this point. The mean diameters of both surface nano-holes and underneath nanotubes increase with increasing potential. The increasing trend of the nanotube diameter is more clearly from bottom view, as shown in Fig. 3 (a2, b2, c2, d2). The diameter increases from 33 to 128 nm. The differences of diameter can be ascribed to the distinct potentials (namely current density). According to Faraday's first law, the

amount of precipitation on the anode is proportional to the current density under a certain time. The thickness of nanoporous layer gradually increases from approximate 0 to 240 nm, indicating that high voltage would reduce the dissolution of as-formed nanoporous layers. The possible explanation is that fluoride ions are more inclined to diffuse along the nanotubes under high potential. Charge transfer happens between interfaces, thus alleviate corrosion on the top of the layer.

For the experiment under different potentials, anodization consisted of two parts - a potential swept from the OCP to desired potentials following potential holding for different time. The potentiodynamic polarization curves from OCP to target potentials with a sweep rate of 50 mVs<sup>-1</sup> and the following current-time curves at fixed potentials for 2 h are shown in Fig. 4.

The curve under each potential was characterized by a behavior with an increase/decrease/increase/decrease sequence. Firstly, the current density gradually increases until the target potential is reached during the potential sweep. Then the current density decreases following by a short increase, and then it decreases again until reaching a steady value. This current density response can be attributed to a high-electrical field oxide formation behavior [19]. Higher anodization potential results in higher steady current density because of higher driving force for the electrochemical formation of oxide layers [21]. The current densities are nearly doubled for each 10 V increase of the potential. For the holding potential of 40 V, the current density at the end of sweeping is not very stable and appears wave-like increasing. In addition, the current-time curve drops sharply at beginning and the increase of current density last a long time. These behaviors are probably correlated to electrochemical process of nanotubes growth under high potential.

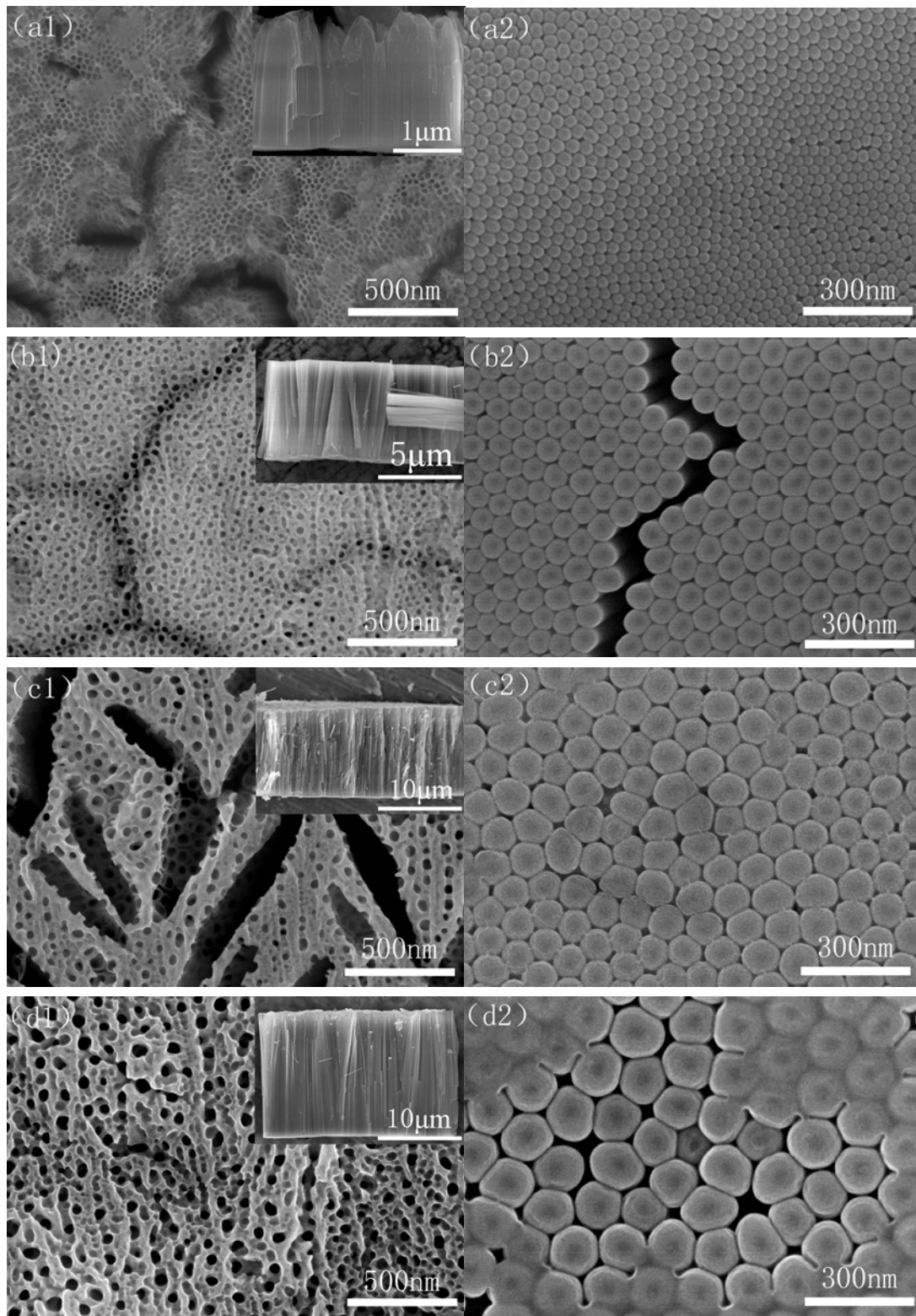


Fig. 3. Top-view (cross-sectional view in insets) and bottom-view SEM images of oxide layers formed on Ti-50Ta (a) 10 V; (b) 20 V; (c) 30 V; (d) 40 V by anodization at 50 °C in 10:90 vol.% of  $H_2O:C_3H_8O_3$  containing 0.3 M  $NH_4F$  for 1 h.

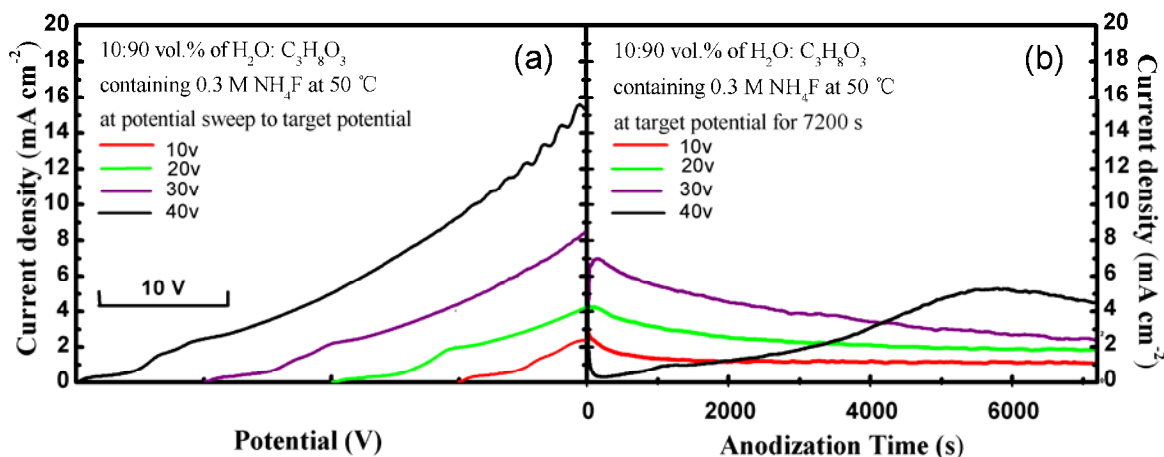


Fig. 4. (a) Polarization curves during the potential sweep from OCP to target potential with a scan rate of  $50 \text{ mVs}^{-1}$  and (b) current-time curves at fixed potential for 2 h in 10:90 vol.% of  $\text{H}_2\text{O} : \text{C}_3\text{H}_8\text{O}_3$  containing 0.3 M  $\text{NH}_4\text{F}$  for Ti-50Ta alloy.

Nanotubes formed under high anodization potential are relative longer and thicker than those formed under low anodization potential, as shown in Fig. 5. Both the diameter and thickness of nanotubes increase almost linearly with increasing anodization potential. As anodization potential increased from 10 to 40 V, the thickness increased from 1.98 to  $14.97 \mu\text{m}$  and the diameter increased from 33 to 128 nm. Combining with the potentiodynamic polarization and current-time curves, it is suggested that the mean diameter and length of the nanotubes were determined by the final sweeping current and the steady current, respectively.

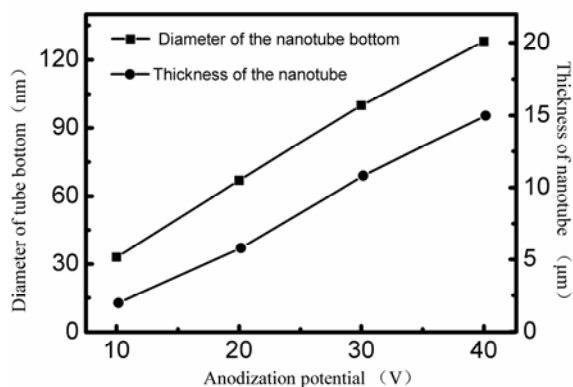


Fig. 5. Dependence of nanotube bottom diameter and nanotube thickness on anodization potential after 1 h at  $50^\circ\text{C}$ .

Fig. 6 shows the XRD patterns of the substrate, the as-formed nanotubes and nanotubes after annealing for 2 h at 450, 600 and  $750^\circ\text{C}$ , respectively. It can be seen only  $\alpha''$  phase was indexed in the patterns of the substrate and the as-formed nanotubes, and only reflections assigned to the substrate occur, indicating that the as-formed

self-organized nanotubes typically have an amorphous structure [16].

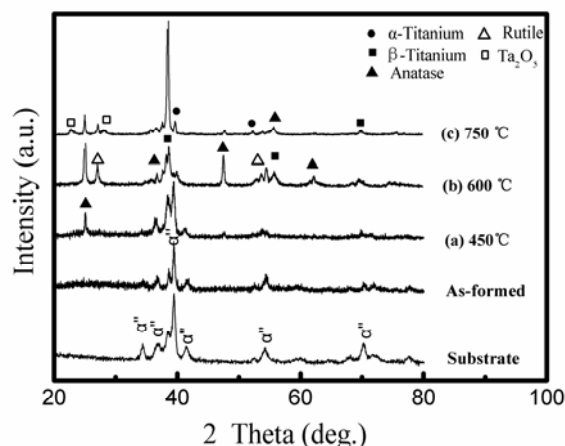


Fig. 6. XRD patterns of the oxide nanotubes formed on the Ti-50Ta alloy substrate after annealing at (a)  $450^\circ\text{C}$ , (b)  $600^\circ\text{C}$  and (c)  $750^\circ\text{C}$  respectively for 2 h.

After annealing at  $450^\circ\text{C}$  for 2 h, the amorphous structure transforms to anatase. This is favorable for its application in biomedical area since crystallinity of the nanotubes possesses more excellent corrosion resistance [23]. At  $600^\circ\text{C}$ , the rutile can be observed, indicating a transformation from anatase to rutile. It is reported that the crystal structure of the nanotubes could be converted under appropriate heat treatment [24, 25]. Tantalumoxide ( $\beta\text{-Ta}_2\text{O}_5$ ) was formed after annealing at  $750^\circ\text{C}$ . The more stable and passive  $\text{Ta}_2\text{O}_5$  can strengthen the initial  $\text{TiO}_2$  layer and improve corrosion resistance when using in biomedical applications [26].

#### 4. Conclusions

In the present work, we investigated the growth of self-organized TiO<sub>2</sub> nanotube layer on Ti-50Ta alloy in 10:90 vol.% of H<sub>2</sub>O: C<sub>3</sub>H<sub>8</sub>O<sub>3</sub> containing 0.3 M NH<sub>4</sub>F. The result indicates that homogenous nanotubular layer can be formed on this alloy under different anodization parameters. Nanotubes with hexagonal arrangement are formed under appropriate voltage 20 V for several hours. Higher potential can alleviate the dissolution of nanoporous layers. The diameter of the nanotubes can be strongly influenced by the applied potential, while length of the nanotubes is determined by the electrolyte temperature and anodizing time. The current density in the experimental process plays a vital important role in the length and diameter of nanotubes. The nanotube layer formed is amorphous in nature, but it can be crystallized by annealing. Especially, Ta<sub>2</sub>O<sub>5</sub> are formed after annealing at 750 °C.

#### Acknowledgements

This work was supported by the Key Projects in the Tianjin Science & Technology Pillar Program (09ZCKFGX29100) and National Natural Science Foundation of China (50901051). The infrastructural supports from the Tianjin University are also acknowledged.

#### References

- [1] Y.T. Liu, X.L. Zhang, R.H. Liu, R.B. Yang, C.B. Liu, Q.Y. Cai, *J. Solid. State. Chem.* **184**, 684 (2011).
- [2] G.K. Mor, K. Shankar, M. Paulose, O.K. Varghese, C.A. Grimes, *Nano. Lett.* **5**, 191 (2005).
- [3] M. Paulose, K. Shankar, O.K. Varghese, G.K. Mor, B. Hardin, C.A. Grimes, *Nanotechnology.* **17**, 1446 (2006).
- [4] C.Y. Chiang, S.H. Chiou, W.E. Yang, M.L. Hsu, M.C. Yung, M.L. Tsai, L.K. Chen, H.H. Huang, *Dent. Mater.* **25**, 1022 (2009).
- [5] V. Zwillling, E.D. Ceretti, A.B. Forveille, D. David, M. Y. Perrin, M. Aucouturier, *Surf. Interface Anal.* **27**, 629 (1999).
- [6] J.M. Macak, K. Sirotna, P. Schmuki, *Electrochim. Acta.* **50**, 3679 (2005).
- [7] J.M. Macak, P. Schmuki, *Electrochim. Acta.* **52**, 1258 (2006).
- [8] M. Steinhart, J.H. Wendorff, A. Greiner, R.B. Wehrspohn, R.B. Wehrspohn, K. Nielsch, J. Schilling, J. Choi, U. Gosele, *Science* **296**, 1997 (2002).
- [9] H. Tsuchiya, J.M. Macak, L. Taveira, P. Schmuki, *Chem. Phys. Lett.* **410**, 188 (2005).
- [10] I. Sieber, H. Hildebrand, A. Friedrich, P. Schmuki, *Electrochem. Commun.* **7**, 97 (2005).
- [11] I. Sieber, B. Kannan, P. Schmuki, *Electrochem. Solid. ST.* **8**, 10 (2005).
- [12] V. Zwillling, M. Aucouturier, E. Darque-Ceretti, *Electrochim. Acta.* **45**, 921 (1999).
- [13] H. Tsuchiya, S. Berger, J.M. Macak, A. Ghicov, P. Schmuki, *Electrochem. Commun.* **9**, 2397 (2007).
- [14] K. Yasuda, P. Schmuki, *Adv. Mater.* **19**, 1757 (2007).
- [15] X.J. Feng, J.M. Macak, P. Schmuki, *Electrochem. Commun.* **9**, 2403 (2007).
- [16] X.J. Feng, J.M. Macak, S.P. Albu, P. Schmuki, *Acta. Biomater.* **4**, 318 (2008).
- [17] H. Tsuchiya, J.M. Macak, A. Ghicov, Y.C. Tang, S. Fujimoto, M. Niinomi, T. Noda, P. Schmuki, *Electrochim. Acta.* **52**, 94 (2006).
- [18] Y.Q. Liang, X.J. Yang, Z.D. Cui, S.L. Zhu, *J. Mater. Res.* **24**, 3647 (2009).
- [19] H. Tsuchiya, T. Akaki, J. Nakata, D. Terada, N. Tsuji, Y. Koizumi, Y. Minamino, P. Schmuki, S. Fujimoto, *Corros. Sci.* **51**, 1528 (2009).
- [20] B. O'Brien, J. Stinson, W. Carroll, *Acta. Biomater.* **4**, 1553 (2008).
- [21] M. Paulose, K. Shankar, S. Yoriya, H.E. Prakasham, O.K. Varghese, G.K. Mor, T.A. Latempa, A. Fitzgerald, C.A. Grimes, *J. Phys. Chem. B.* **110**, 16179 (2006).
- [22] J.M. Macak, H. Hildebrand, U.M. Jahns, P. Schmuki, *J. Electroanal. Chem.* **621**, 254 (2008).
- [23] H.H. Park, I.S. Park, K.S. Kim, W.Y. Jeon, B. K. Park, H.S. Kim, T.S. Bae, M.H. Lee, *Electrochim. Acta.* **55**, 6109 (2010).
- [24] S.H. Jang, H.C. Choe, Y.M. Ko, W.A. Brantley, *Thin Solid Films.* **517**, 5038 (2009).
- [25] H. Jha, R. Hahn, P. Schmuki, *Electrochim. Acta.* **55**, 8883 (2010).
- [26] Y.L. Zhou, M. Niinomi, T. Akahori, H. Fukui, H. Toda, *Mat. Sci..Eng. A-struct.* **398**, 28 (2005).

\*Corresponding author: xjyang@tju.edu.cn